Electronic Supplementary Information

4.4 V supercapacitors based on super-stable mesoporous carbon sheet made of edge-free graphene walls

Keita Nomura, Hirotomo Nishihara, Naoya Kobayashi, Toshihiro Asada, and Takashi Kyotani*

1. Experimental Section

1.1. Materials

rGO (Sigma-Aldrich) and GF (G-49, EMJapan Co., Ltd.) were purchased, while SWCNT (SG101, ZEON Corp., diameter is 3–5 nm) and AC (Kuraray Chemical Co., Ltd.; YP-50F) were kindly provided from the suppliers.

GMS powder was prepared based on the method we have reported,[1] with a modification for scale-up. About 12 g of γ-alumina nanoparticles (TM-300, Taimei Chemicals Co., LTD.) was mixed with 40 g of quatz sand (Wack Pure Chemical Industries, Ltd.), and the mixture was stuffed into a home-made quartz capsule (cylinder shape; φ 48 mm × 158 mm). The both ends of the capsule are porous quartz filters. The capsule was then placed inside a holisontal quartz tube, and CVD (20 vol%-methane/Ar, 900 °C for 2 h) was performed. After cooling down the sample, the capsule was replaced inside the quartz tube with exchanging its direction, and the same CVD was performed from the opposite side of the capsule. The carbon-coated alumina nanoparticles are separated from the quartz sand by sieving, and alumina template was removed by chemical etching with HF. The resulting mesoporous carbon, carbon mesosponge (CMS), was then annealed at 1800 °C for 1 h under a reduced pressure (Ar atomosphere, 10 Pa) to increase the crystallinity. GMS powder was thus obtained.

GMS sheet was prepared as follows. γ-alumina nanoparticles (TM-300, Taimei Chemicals Co., LTD.) were pressed with a graphite mold into a sheet shape (9 cm × 4 cm × 0.2 mm) at room temperature under 10 MPa for a few seconds. An upside mold is removed, and the Al_2O_3 sheet placed in a downside mold was subjected to CVD (15 vol%-methane/Ar, 900 °C for 3 h) for carbon coating of the porous Al_2O_3 sheet. The resulting sample (C/Al_2O_3 sheet) was carefully immersed into HF solution (9.2%) to remove Al_2O_3 to obtain a CMS sheet, and it was subjected to a high-temperature treatment at 1800 °C for 1 h under a reduced pressure (Ar atomosphere, 10 Pa) to increase its crystallinity. A GMS sheet was thus obtained.

1.2. Characterization

Morphology of the samples was observed by a scanning electron microscope (SEM:S-4800, Hitachi, Ltd.) and a transmission electron microscope (TEM: JEM-2010, JEOL Ltd.). Powder XRD patterns of the samples were recorded with an X-ray diffractometer (MiniFlex600, Rigaku Co.) with Cu Kα radiation generated at 40 kV and 15 mA. Nitrogen physisorption measurements were carried out at −196 °C using a volumetric sorption analyzer (BEL Japan, BELSORP MAX). The specific surface area (S_{BET}) was calculated by the BET method in the pressure range of P/P_0 = 0.05–0.35. Only for microporous carbons, P/P_0 = 0.01–0.05 was applied.[2] Total pore volume was calculated from the amount adsorbed at P/P_0 = 0.96. The mesopore size distribution was calculated by using the Barrett–Joyner–Halenda (BJH) method applied to the N_2 adsorption isotherm. The electric conductivity of an electrode sheet was measured by a four-probe technique with Loresta-GP MCP-T610 equipment (Mitsubishi Chemical Co.). For rGO, AC, and GMS powder, their electrode sheets are formed on a Si

wafer (> 1000 Ω cm). The air-oxidation stability was examined by a TG analyzer (Shimadzu DTG-60H or TGA-51H) under an air flow. Raman spectra were measured with a Jasco NRS-3300FL spectrometer with the 532.2 nm line. The intensity was normalized by the G-band. To estimate the number of edge sites, we adopted a special TPD analysis reported elsewhere.[3] Our group has developed an advanced TPD system which reaches a temperature of 1800 °C, capable of precisely determining the total gas evolution of any type of carbon material.[3]

1.3. Electrochemical measurement

Two-electrode symmetrical cell was assembled in the following manner. For rGO, AC, and GMS powder, the sample was mixed with CB (Denka black, Denki Kagaku Kyogyo Co., Ltd.) as conductive additive and binder polymer (carboxymethylcellulose (CMC), (WS-C, DKS Co. Ltd.) dissolved in water) to obtain a homogeneous slurry. Then, isopropyl alcohol was added to adjust the viscosity, followed by mixing with the second binder polymer (acrylate-based polymer (ABP) (AZ-9129, ZEON Corp.) dissolved in water). The resulting slurry was pasted on a current collector (Al foil coated with diamond-like carbon, provided by TOC capacitor Co., Ltd.). After dried up at 60 °C, the foil was cut out to be a working electrode (circular shape, diameter is 16 mm). The composition of the working electrode is shown in Table S1. After additional drying at 100 °C under vacuum for 12 h, two working electrodes are packed in a 2032-type coin cell together with a cellulose separator (TF4850, Nippon Kodoshi Co.) and an electrolyte: 1.5 M TEMA-BF_4/PC in Ar. SWCNTs were dispersed in N-methylpyrroridone, and the resulting dispersion solution was filtrated under vacuum to obtain a freestanding sheet. GF and GMS sheet as well as the SWCNT sheet were directly used as self-standing electrode sheet. These sheets are cut into 1×1 cm and simply attached to the current collector without using binder polymers.

A harsh stability test was carried out by continuously loading 3.5 V to a two-electrode cell placed inside an oven kept at 60 °C. To check the change of capacitance, the cell was temporarily taken out from the oven to be cooled down to 25 °C, and Galvanostatic charge/discharge curves were measured within 0–3.5 V. After the capacitance measurement, the cell was again subjected to the high voltage and temperature to continue the stability test. After the stability test, the cell was disassembled and a positive electrode and a negative electrode were washed with propylene carbonate, and then dried at 100 °C for 24 h under vacuum. Then, each of the electrodes was subjected to N_2 adsorption-desorption measurement (–196 °C) and SEM observation.

The energy density (E [J g^{-1}]) of EDLC can be calculated by the equation (1) which is shown in the main text:

$$E = \frac{1}{2} CV^2 \qquad (1)$$

where C and V are capacitance [F g^{-1}] and operation voltage [V] in EDLC. E is obtained with the unit of J g^{-1}, and it is converted into commonly used appearange, E' [Wh kg^{-1}], by the following relation.

$$E' = \frac{1}{3.6} E \qquad (2)$$

In this work, the energy density is calculated based on the total electrode mass (including CB and binder polymers) in positive and negative electrodes.

The charge/discharge measurement was then performed by using Bio-Logic VMP3 with several different current densities. Specific capacitance, C [F g^{-1}], was calculated by the following equation:

$$C = \frac{i\Delta t}{m\Delta V} \qquad (3)$$

where i, Δt, m, and ΔV are current [A], time of discharge [s], the total mass of carbon included in both electrodes [g], and working voltage [V]. By using the equations (1), (2), and (3), the energy density, E' [Wh kg^{-1}], can be calculated from a discharge curve. During the discharge measurement, VMP3 records the power, P [W], and it becomes maximum at the beginning of the discharge measurement. By using the maximum power, P_{max}, the power density, P' [W kg^{-1}], based on the electrode mass was calculated by the following equation:

$$P' = \frac{P_{max}}{m/1000} \qquad (4)$$

Thus, Ragone plots was obtained, as shown in Figure 5d.

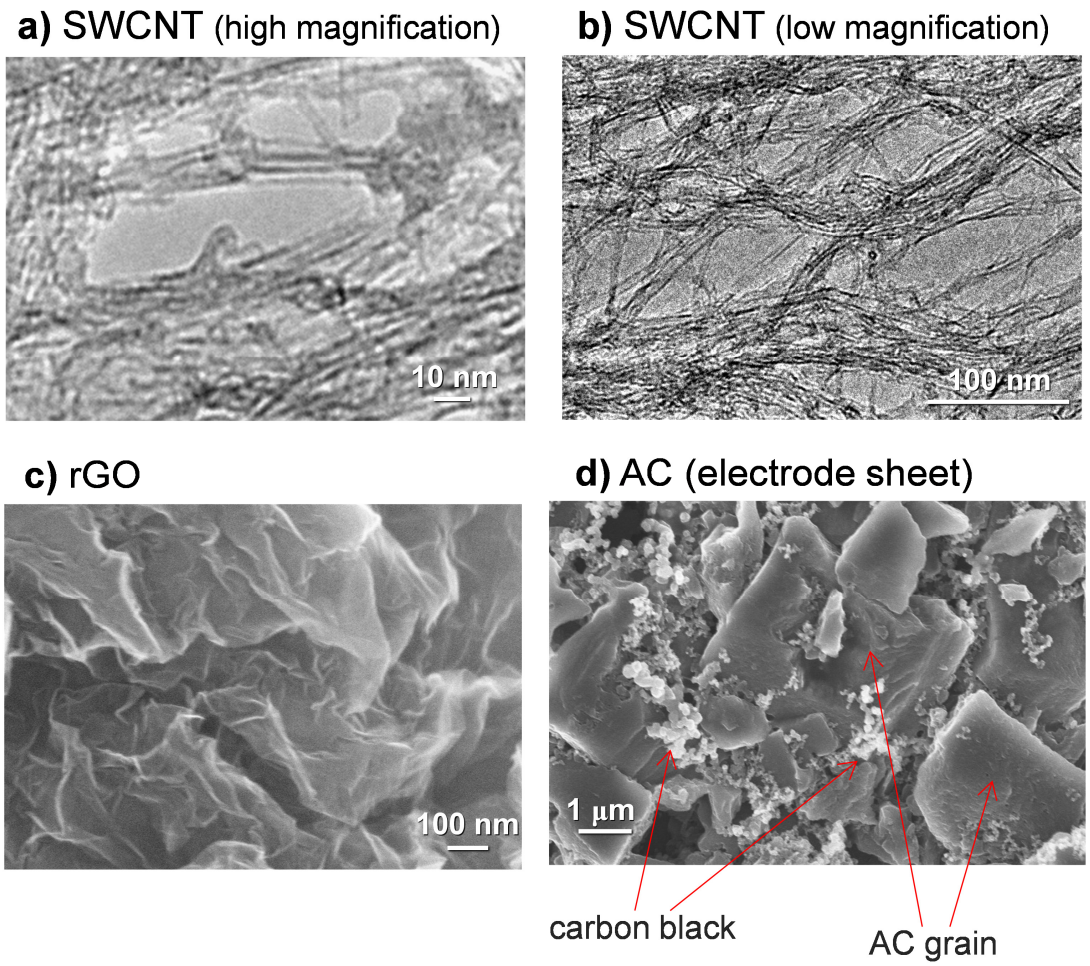

Figure S1. (a,b) TEM images of SWCNTs. The diameter is about 3–5 nm. Bundling is observed in (b). (c) SEM image of rGO. Wrinkled sheets are observed. (d) SEM image of an AC electrode. In addition to AC grains, carbon black can be observed as aggregated small spheres. It is hard to recognize binder polymers by SEM.

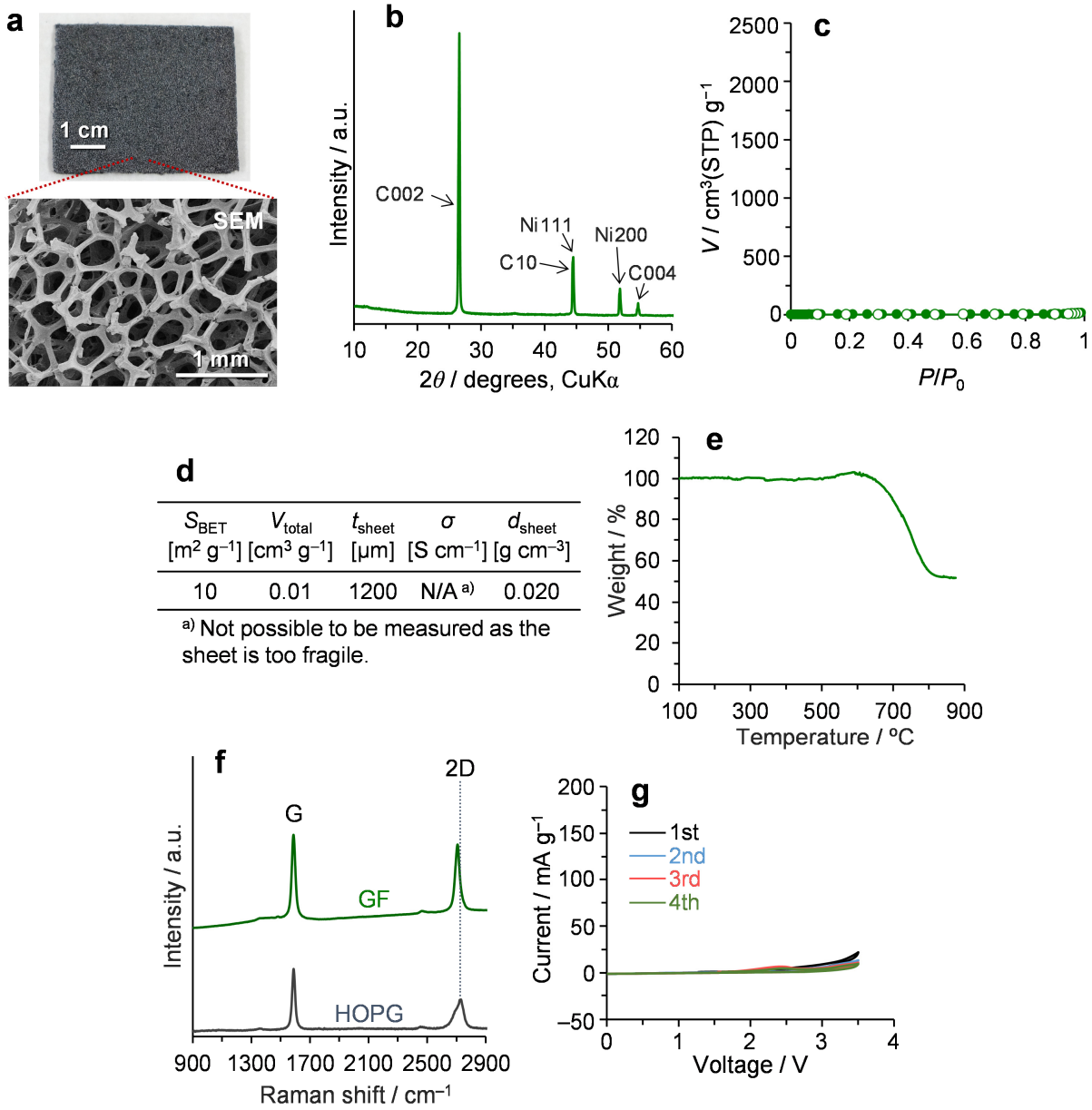

Figure S2. Characterization results on graphene foam (GF). (a) Photo of GF (top) and its SEM image (bottom). GF is prepared by using a Ni foam as a template, and therefore, possesses a 3D continuous network structure. (b) XRD pattern. (c) N_2 adsorption-desorption isotherm (−196 °C). (d) A table of the property of GF, corresponding to Table 1. (e) TG curve measured in air. (f) Raman spectra of GF and HOPG. The 2D peak position of HOPG is indicated with a grey dashed line. (g) Change of wide-range (0–3.5 V) CV patterns from the 1st to the 4th cycle. GF sheet is directly used as a working electrode.

The XRD pattern (b) shows very sharp carbon 002, 10, and 004 peaks, indicating the developed graphene stacking structures which give rise to very poor porosity (c and d). Moreover, GF shows the peaks of Ni metal (b), and the amount is great as found from its thermogravimetric (TG) curve measured in air (e). Another problem is its large pore size (a; ~ 200 nm), resulting in a very low sheet density (d; 0.02 g cm^{-3}). The 2D-band of GF is less intense than its G-band (f), and its position is very close to that of HOPG, indicating that GF consists of not single-layer graphene but stacked ones, as already described. Moreover, GF shows a very small capacitance (g) because of its poor porosity. Thus, the commercial GF is found not to be suitable for supercapacitor application.

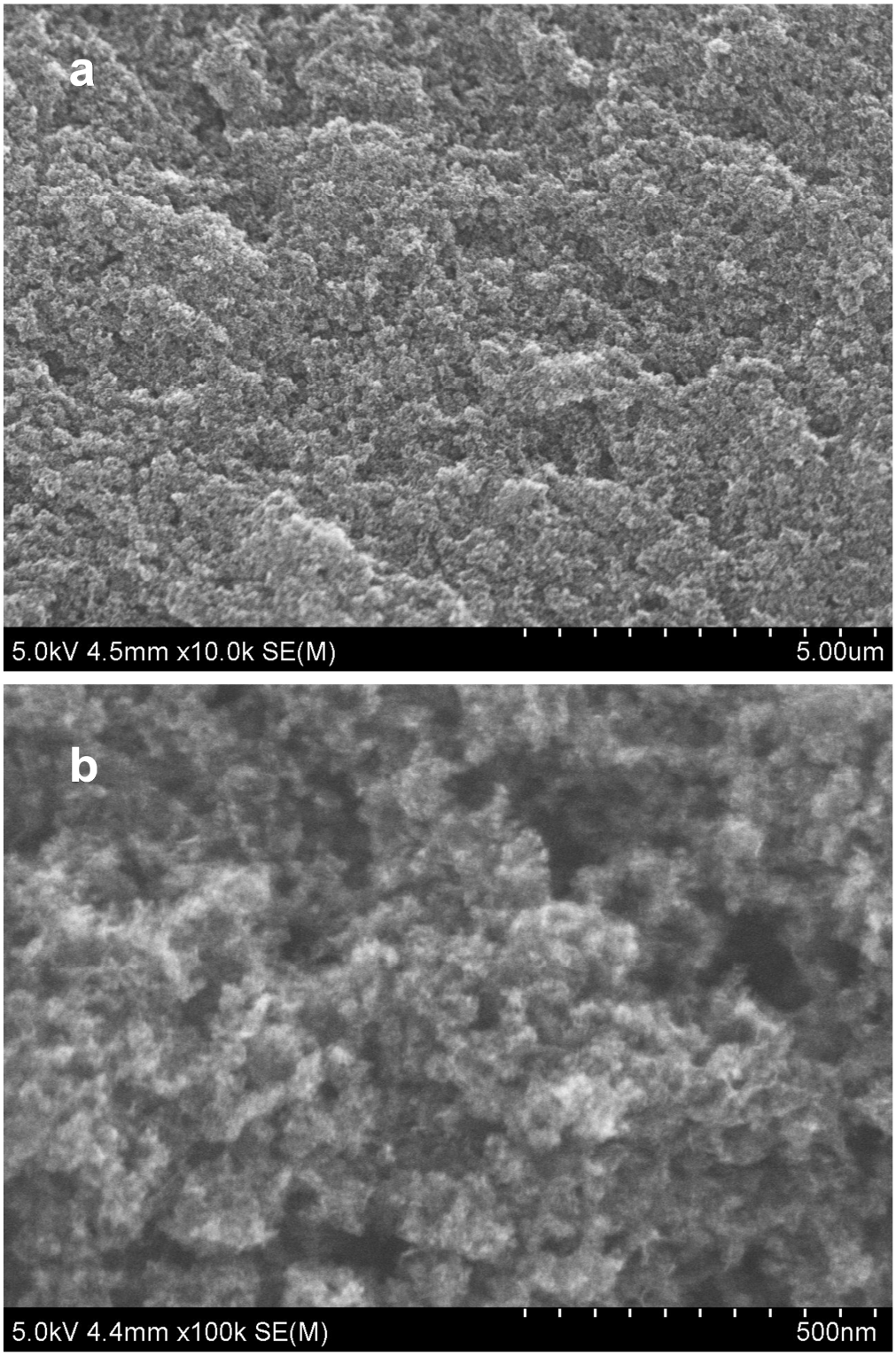

Figure S3. SEM images of GMS sheet with (a) low and (b) high magnifications. There are many pores larger than 20 nm, which accords to the mesopore-size distribution (Fig. 2c).

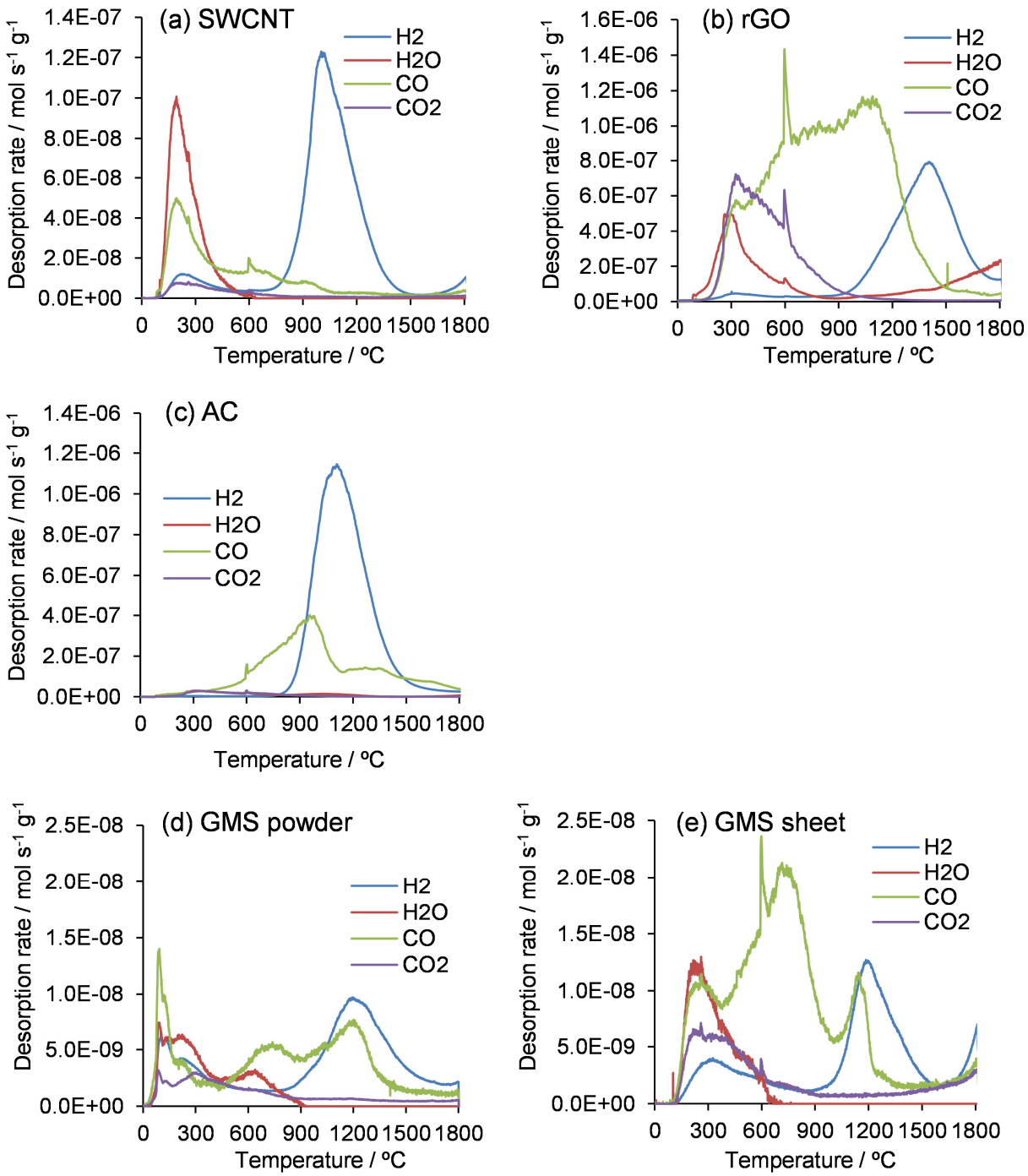

Figure S4. Gas (H_2, H_2O, CO, and CO_2) evolution patterns of (a) SWCNTs, (b) rGO, (c) AC, (d) GMS powder, and (e) GMS sheet, during the TPD experiment. The temperature of the sample is measured with a radiation thermometer equipped with three different detectors for different temperature ranges: below 260 °C, 260–600 °C, and above 600 °C. At 260 °C and 600 °C, a detector switches to another, and this causes a momentary stagnation of temperature rize, resulting in the appearance of sharp peaks at these temperatures. Nevertheless, these noises do not matter for the estimation of the total gas evolution amount. It is very clear that gas evolutions in rGO and AC are much more significant than those of SWCNTs and GMSs. The amount of the total gas evolution (H_2, H_2O, CO, and CO_2) represents the amount of carbon edge sites which are terminated with H and oxygen-functional groups. The TPD results clearly demonstrates the edge-free nature of GMSs.

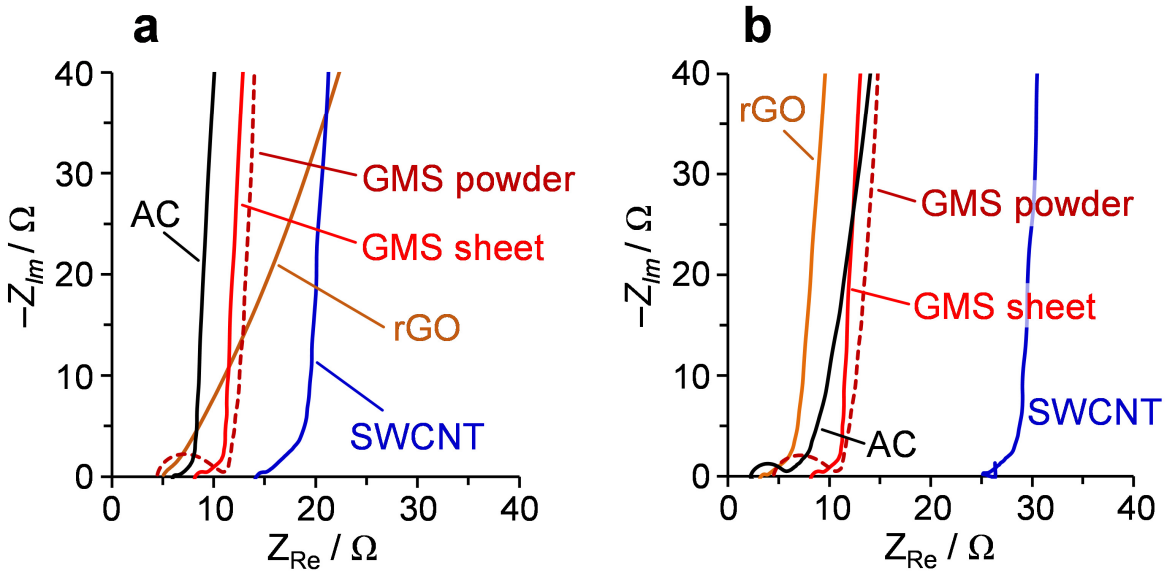

Figure S5. Nyquist plots of the samples (a) before and (b) after the measurements of CV (four cycles within 0−3.5 V at 1 mV s^{-1}) and GC curves (four cycles within 0−3.5 V at 50 mA g^{-1}, based on the mass of active material in a positive elctrode) at room temperature. The EIS spectra of AC, rGO, and SWCNTs are noticeably changed, indicating the occurrence of irreversible structure changes in these electrodes. The EIS spectra of GMS powder and sheet are almost unchanged, indicating their excellent stability even after a severe polarization up to 3.5 V.

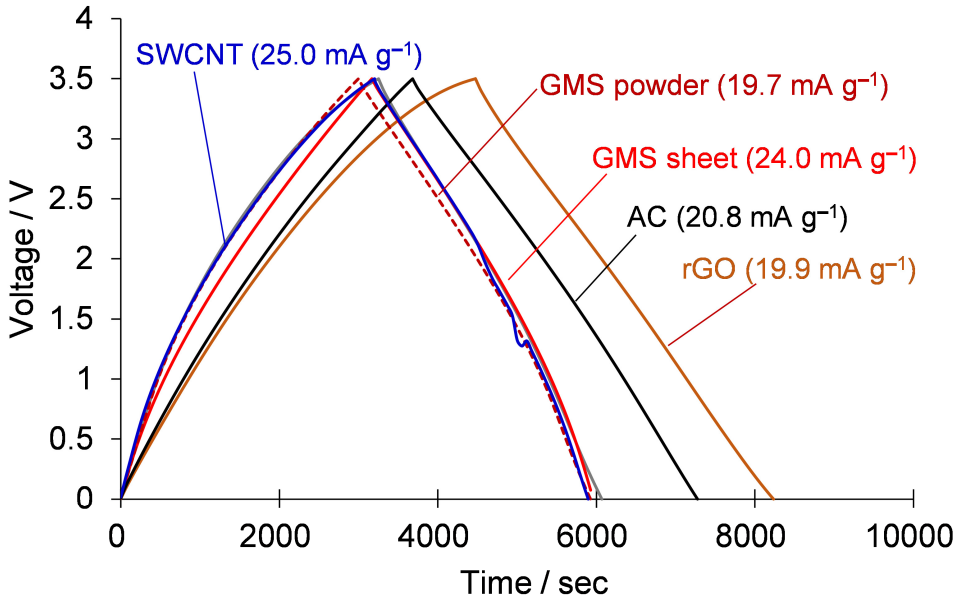

Figure S6. Galvanostatic charge-discharge curves masured with a two-electrode cell in 1.5 M TEMA-BF_4/PC at 25 °C. Current density (mA g^{-1}) was adjusted to be 50 mA g^{-1} based on the active mass (exluding CB and binder polymers) of a positive electrode. In the above graph, current densities based on the total electrode mass (including CB and binder polymers) are shown in parentheses. Note that capacitance (C_{two}) is calculated based on the total electrode mass in this work.

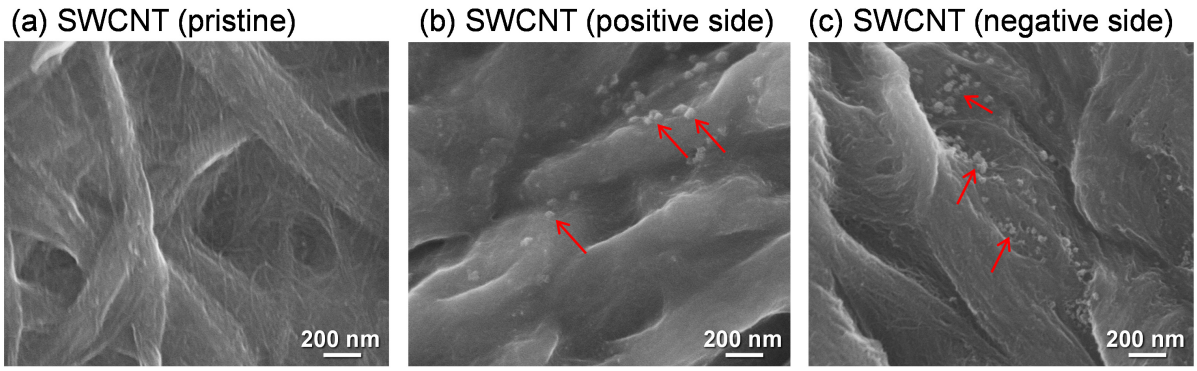

Figure S7. SEM images of electrode sheets of SWCNTs before (pristine) and after (both positive and negative electrodes) the harsh stability test. (a) The pristine sample before the stability test. (b) The positive electrode after the stability test. (c) The negative electrode after the stability test. At the surface of the pristine SWCNTs (a), its fibrous structure is observed. However, the surfaces after the stability test (b,c) such fibrous structure is hard to be observed, probably because of the deposition of solid products. Moreover, apparent solid deposition is observed in both electrodes, as indicated by arrows.

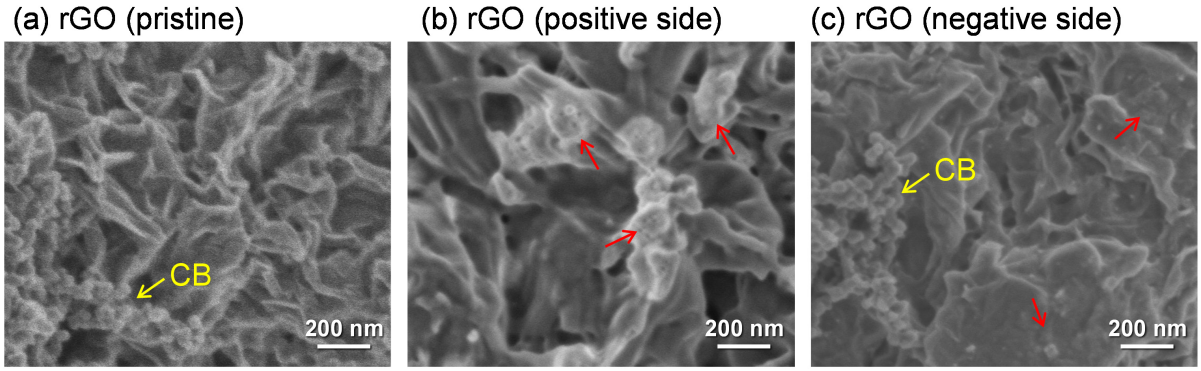

Figure S8. SEM images of electrode sheets of rGO before (pristine) and after (both positive and negative electrodes) the harsh stability test. (a) The pristine sample before the stability test. (b) The positive electrode after the stability test. (c) The negative electrode after the stability test. The electrode sheet of rGO contains CB, as observed in (a). In (b), CB is hard to be find, and many deposites indicated by arrows are observed, apparently showing the formation of solid products. In (c), CB can be found, but the surface of rGO becomes rougher, as indicated by arrows, indicating the formation of solid products, too.

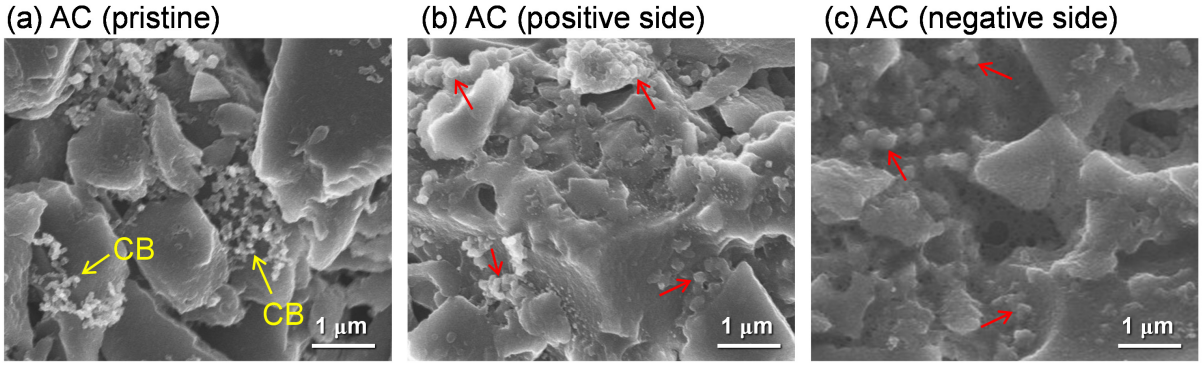

Figure S9. SEM images of electrode sheets of AC before (pristine) and after (both positive and negative electrodes) the harsh stability test. (a) The pristine sample before the stability test. (b) The positive electrode after the stability test. (c) The negative electrode after the stability test. The electrode sheet of AC contains CB, as observed in (a). In both (b) and (c), CB is hard to be find, and many deposites indicated by arrows are observed, apparently showing the formation of solid products.

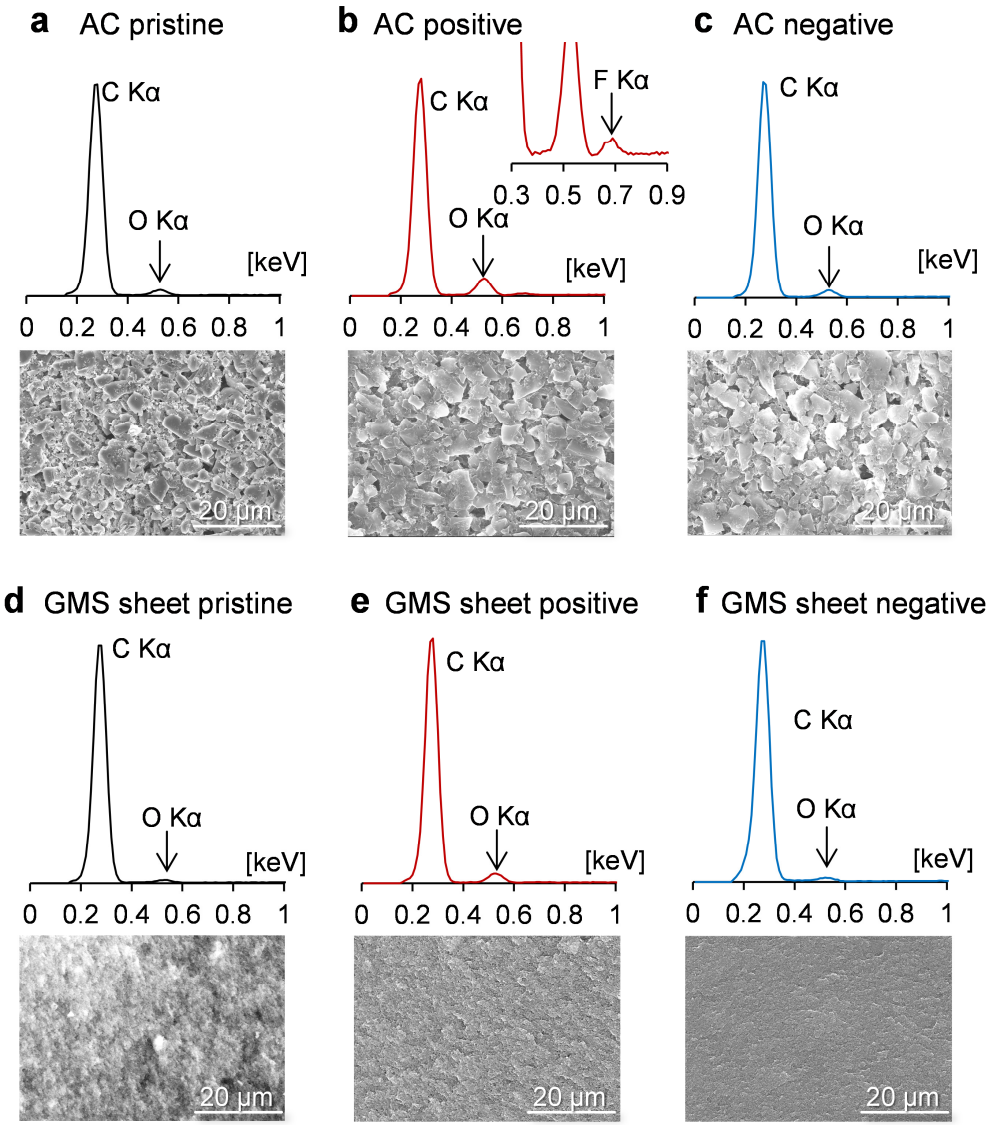

Figure S10. EDX spectra and SEM images for (a-c) AC and (d-f) GMS sheet: (a, d) shows the data of the pristine electrodes, while (b, e) and (c, f) are the data of the positive and negative electrodes, respectively, after the harsh stability test in which a cell is kept at 60 ºC with loading a high voltage of 3.5 V (Fig. 4). In the positive electrode of AC, the increase of O and F is observed (b), as Ishimoto *et al.* have reported.[4] In GMS sheet, the increase of O and F is much less (e) compared to the case of AC.

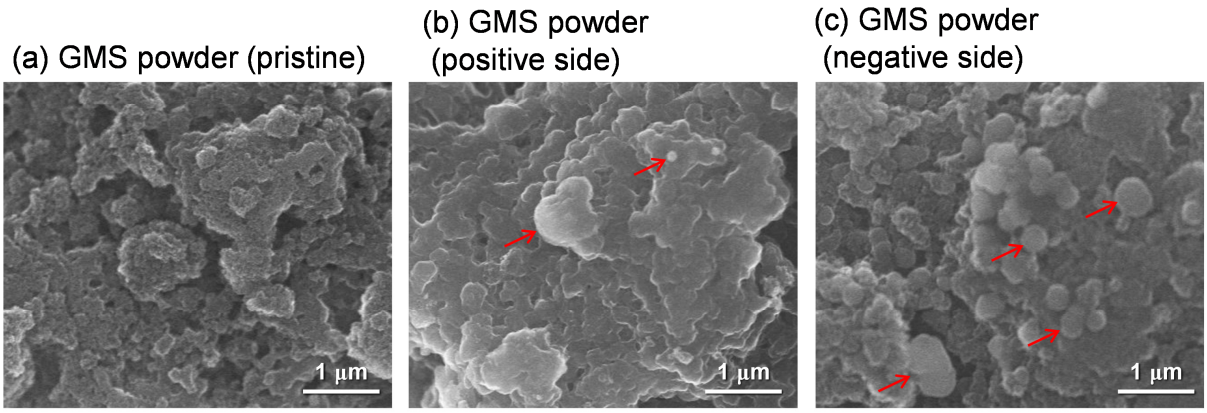

Figure S11. SEM images of electrode sheets of GMS powder before (pristine) and after (both positive and negative electrodes) the harsh stability test. The electrode was prepared by the same manner as that for other samples with the composition of sample:CB:CMC:PAA = 80:0:15:5. (a) The pristine sample before the stability test. (b) The positive electrode after the stability test. (c) The negative electrode after the stability test. In both (b) and (c), apparent solid products are observed as indicated by arrows. Thus, deposition of the solid products is inevitable even in GMS when it is a powder form and does not have long range 3D continuous structure.

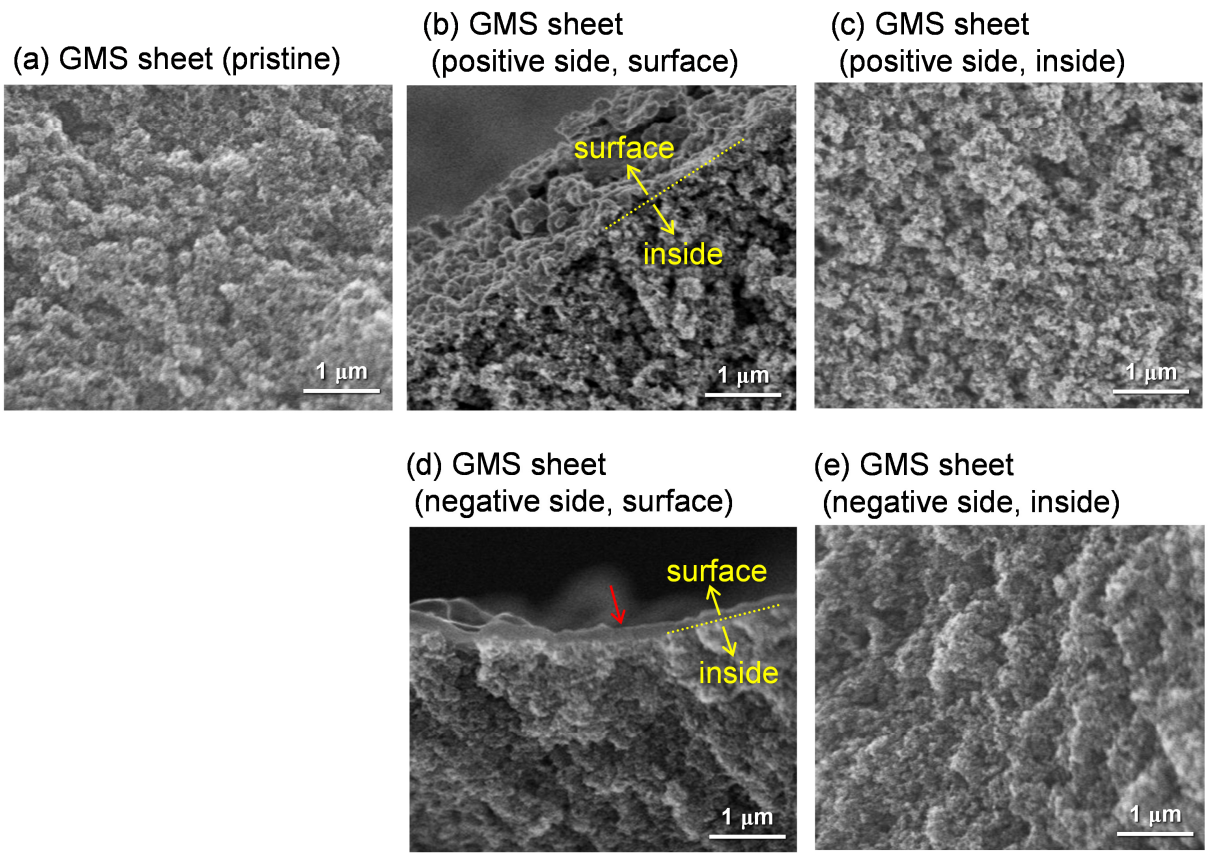

Figure S12. SEM images of GMS sheets before (pristine) and after (both positive and negative electrodes) the harsh stability test. (a) The pristine sample before the stability test. (b,c) The positive electrode after the stability test. (b) Outside surface, and (c) inside the sheet. (d,e) The negative electrode after the stability test. (d) Outside surface and (e) inside the sheet. A small amount of deposition (indicated by a red arrow) is observed only at the surface of the negative electrode sheet (d). Unlike other samples, no apparent change is observed inside the sheet (c,e), indicating suppressed formation of solid product in GMS sheet.

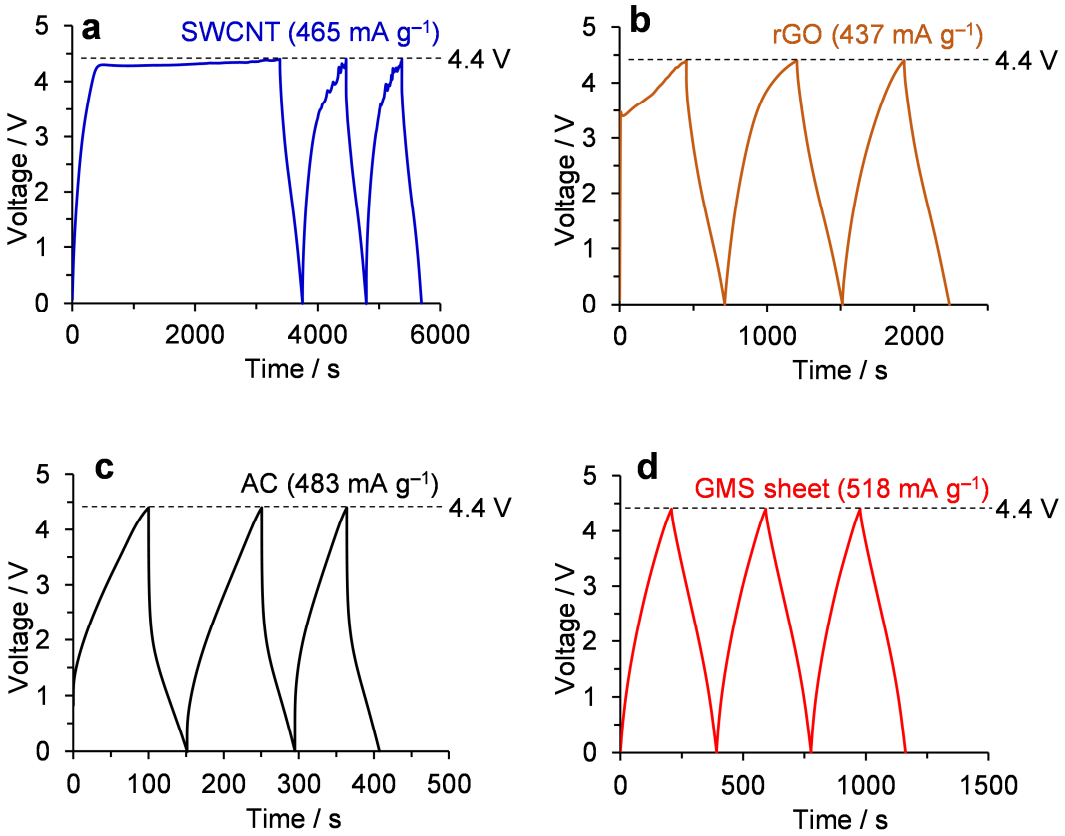

Figure S13. Galvanostatic charge-discharge curves of (a) SWCNTs, (b) rGO, (c) AC, and (d) GMS sheet, masured with a two-electrode cell in 1.5 M TEMA-BF_4/PC at 25 °C. Current density (mA g^{-1}) was adjusted to be 1 A g^{-1} based on the active mass (exluding CB and binder polymers) of a positive electrode. In each graph, current density based on the total electrode mass (including CB and binder polymers) is shown in parentheses. Note that capacitance (C_{two}) is calculated based on the total electrode mass in this work.

Figure S14. A photo of the broken cell made by SWCNTs after 500 cycles of charge-discharge measurement in the voltage range of 0–4.4 V.

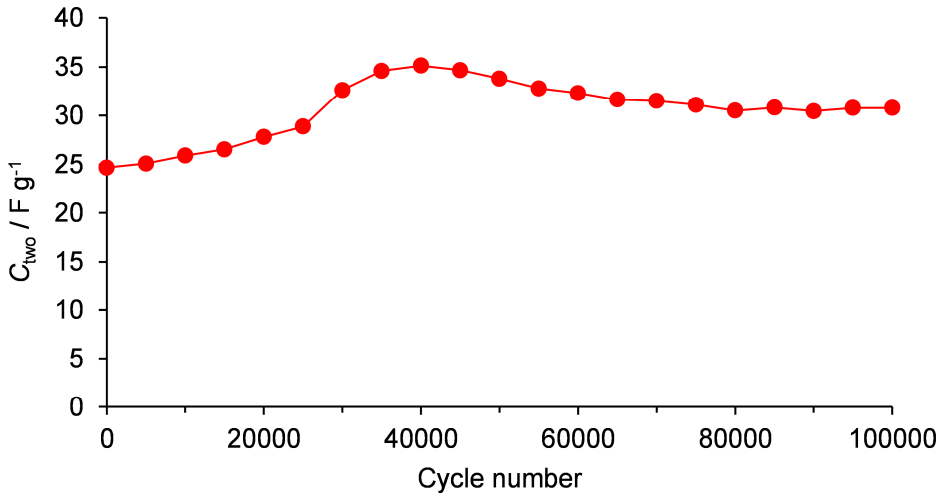

Figure S15. Long-term stability test for 100000 cycles on GMS sheet. A symmetric coin cell was assembled and galvanostatic charge-discharge cycling was performed with a potential range of 0 to 4.4 V at 25 °C. Current density applied was 46 A g^{-1} (based on the total mass of GMS sheet included in the coin cell). At every 5000 cycles, 0.46 A g^{-1} was applied to check the precise capacitance.

Table S1. Composition of electrode sheet.

Sample name	Sample (wt%)	CB (wt%)	CMC (wt%)	PAA (wt%)
SWCNT	100	0	0	0
rGO	86	5	5	4
AC	88	5	3	4
GF	100	0	0	0
GMS powder	80	0	15	5
GMS sheet	100	0	0	0

References

1. H. Nishihara, T. Simura, S. Kobayashi, K. Nomura, R. Berenguer, M. Ito, et al., *Adv Funct Mater*, 2016, **26**, 6418-6427.
2. C. Ishii and K. Kaneko, *Prog Org Coat*, 1997, **31**, 147-152.
3. J. Takashiro, Y. Kudo, S. J. Hao, K. Takai, D. N. Futaba, T. Enoki, et al., *Phys Chem Chem Phys*, 2014, **16**, 21363-21371.
4. S. Ishimoto, Y. Asakawa, M. Shinya and K. Naoi, *J. Electrochem. Soc.*, 2009, **156**, A563-A571.